

## Raman study of free-standing porous silicon

H. Tanino,\* A. Kuprin,† and H. Deai‡

*Electrotechnical Laboratory, Tsukuba, Ibaraki 305, Japan*

N. Koshida

*Division of Electronic and Information Engineering, Faculty of Technology, Tokyo University of Agriculture and Technology, Koganei, Tokyo 184, Japan*

(Received 3 March 1995; revised manuscript received 31 July 1995)

We have measured Raman spectra of free-standing porous silicon at 10 K. Porous silicon samples were prepared in aqueous and ethanoic electrolytes and the scattering was measured in the range of one- through four-phonon processes. A quantum size effect is clearly observed in the spectral change of the first- and second-order scattering from optical phonons but the scattering of higher orders is much more sensitive to the decrease of nanocrystallite size. The microscopic morphological changes from Si single crystals are discussed.

### INTRODUCTION

It has been determined that when crystalline Si is anodized in dilute aqueous HF solutions at moderate current densities, a porous Si (PS) layer is uniformly formed on the Si substrate.<sup>1,2</sup> The PS layer consists a great number of *micropore* arrays, and can be prepared with porosities in the range 20–80 %. The pore morphology and width (2–50 nm in mean diameter) vary with the anodization variables, the substrate resistivity, and the conduction type. Studies of PS to date have focused on structural,<sup>3–11</sup> material,<sup>12–17</sup> mechanical,<sup>18</sup> interfacial,<sup>19–23</sup> and photoelectrochemical<sup>24–28</sup> properties. Information about the electronic and optoelectronic properties of PS is very important, since there is a possibility that quantum size effects appear in PS. Some evidence of quantum size effects in Si-based materials was reported recently by several authors.<sup>29–32</sup> For PS, in particular, Canham<sup>31</sup> has demonstrated emission of visible (red) photoluminescence from high-porosity Si which was prepared by chemical dissolution (immersion in a HF solution for several hours) of anodized PS. Systematic studies are required to determine the microscopic mechanism of electronic and photonic properties in PS.<sup>29</sup>

Raman-scattering studies of materials give us information about structure, bonding, and disorder. Room-temperature Raman spectra from porous Si films on silicon substrates<sup>33–37</sup> and from free-standing layers<sup>38,39</sup> have been reported. Micro-Raman-scattering spectra at room temperature have also been reported.<sup>40,41</sup> However, except for the work of Mündler *et al.*,<sup>42</sup> and extensive higher-order Raman study of *free-standing* PS has not been performed. In this paper, we report the experimental Raman study of free-standing PS films at low temperature. Without the overlapping Raman signal from the Si substrates, as reported in Refs. 34 and 38, good quality Raman spectra can be easily observed.

### EXPERIMENTAL

The silicon wafers used in these experiments were nondegenerated *p*-type (10–20  $\Omega$  cm) single crystals with a (111)

mirror surface. Before anodization, the wafers were cleaned, an Ohmic contact was formed on the back side, and then the parts of the wafers not to be anodized were covered with an acid-proof wax. The samples were formed by anodization of these wafers in a 50% HF solution using Pt as a counter-electrode at a constant current density of 10 mA/cm<sup>2</sup> for 60 min. At the end of the process the anodization current was increased abruptly up to 300–400 mA/cm<sup>2</sup> to separate the porous layer from the substrate. The porous Si films were then rinsed in pure ethanol and dried in a vacuum chamber. Aqueous 50% HF was used for sample 1, and ethanoic 50% HF was used for sample 2. The porosity and thickness of both resulting PS films were about 65% and 60  $\mu$ m, respectively. Prior to the Raman-scattering experiments the samples were stored for several weeks at ambient atmosphere. The details of the experiment are presented elsewhere.<sup>43,44</sup> The thickness of the probed layer was estimated to be 6  $\mu$ m after correcting the absorption coefficient<sup>45</sup> for the decrease in density and temperature.<sup>46</sup> Measurements of the spectra from porous Si were performed with the incident laser beam collimated to a spot 20  $\mu$ m in diameter at the sample surface, which resulted in a maximum power density of about 1300 W/cm<sup>2</sup>.

### RESULTS

Figures 1 and 2 show the Raman spectra of porous Si samples 1 and 2, respectively, at 10 K for (a) polarization of the incident light  $E_i$  and polarization of the scattered light  $E_s$  parallel to each other,  $E_i \parallel E_s$ ; and (b) perpendicular to each other,  $E_i \perp E_s$ . The labels of peaks A, B, C, etc. correspond to the notations of the features in the Raman spectra of bulk Si(111).<sup>47</sup> For spectral features which were not paid much attention in previous studies, we introduced Greek letters  $\gamma$ ,  $\eta$ ,  $\iota$ , etc. Raman spectra taken from the initial Si(111) substrates are presented for comparison in Fig. 3. Assignment of the spectral features to multiphonon modes is shown in Table I and discussed in detail elsewhere.<sup>44</sup> The Raman signal from PS is much stronger than from the initial substrate. The intensity of the first-order scattering which is due to the optical (*O*) phonons at the center  $\Gamma$  point of the Brillouin zone (BZ),

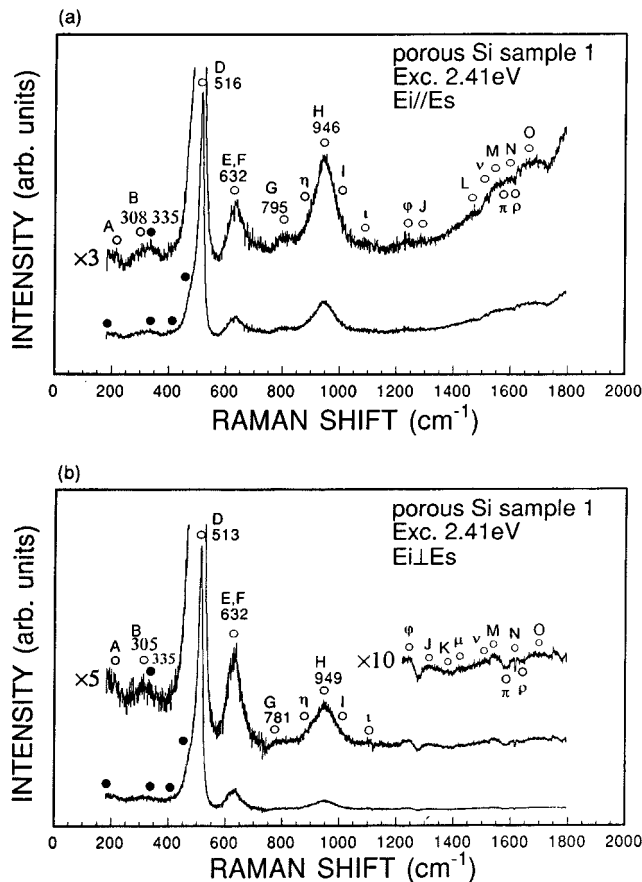


FIG. 1. Raman spectra of porous silicon prepared in an aqueous electrolyte obtained at 10 K for (a) polarization of the incident light  $E_i$  and polarization of the scattered light  $E_s$  parallel to each other,  $E_i \parallel E_s$ ; and (b) perpendicular to each other,  $E_i \perp E_s$ . Open circles indicate features arising from crystalline material, and closed circles show those characteristic of amorphous material.

$O(\Gamma)$  (peak  $D$ ), is much stronger in comparison with that from the initial Si wafer. Intensification of the scattering is extremely high for sample 2. Table II summarizes data on the enhancement of scattering from porous silicon samples. Besides the intensity, there are a number of readily apparent differences between the spectra of the PS samples and that of the  $c$ -Si(111) sample.

In Fig. 4(a) we compare in detail the first-order scattering with  $E_i \parallel E_s$ . Spectral parameters are summarized in Table III. The spectra of the porous Si samples can be characterized by a shift of this peak from its bulk  $c$ -Si position  $\Delta w$  and also by a broadening described by full width at half maximum (FWHM). The peak from sample 1 is very asymmetric, with a tail on the low-energy side extending to  $420 \text{ cm}^{-1}$ . The peak for sample 2 is more symmetric, but a shoulder on its low-energy side extending to a relatively flat and wide plateau is also present. In the  $E_i \perp E_s$  configuration [Fig. 4(b)], the shape and spectral characteristics of the first-order peak from sample 1 are very similar to that of  $E_i \parallel E_s$ . In contrast, sample 2 exhibits bulklike characteristics with a small shift to low energy and only a slight broadening. However, a very tiny shoulder on its low-energy side at around  $470 \text{ cm}^{-1}$  could also be observed [Fig. 2(b)].

For bulk Si, the first-order scattering consists of only  $\Gamma'_{25}$  irreducible symmetry component.<sup>48</sup> A variation in the

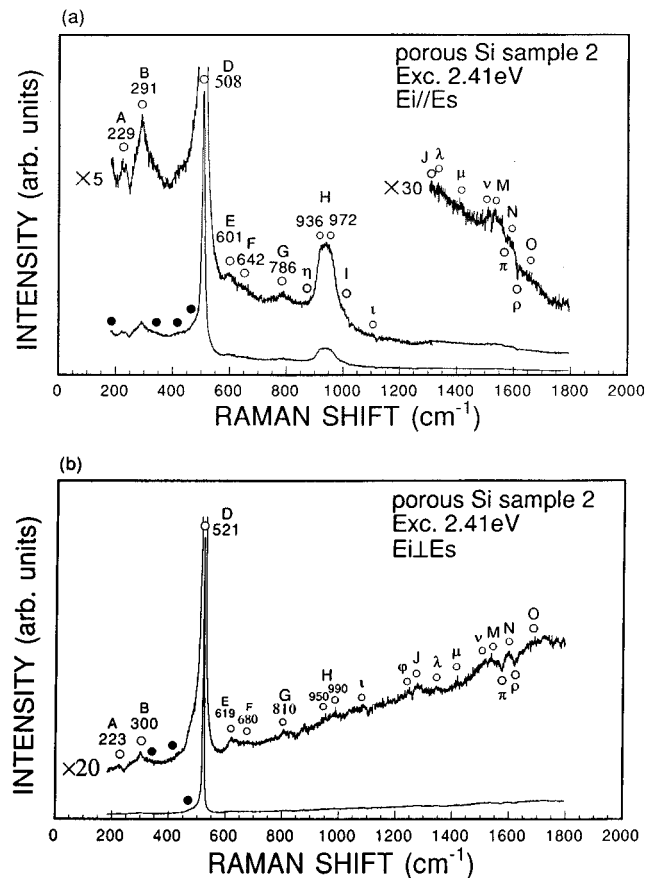


FIG. 2. Raman spectra of porous silicon prepared in an ethanoic electrolyte obtained at 10 K for (a)  $E_i \parallel E_s$  and (b)  $E_i \perp E_s$ . Notations are the same as in Fig. 1.

intensity ratio introduced for peak  $D$ ,  $\rho_D$ , of the scattering in the  $E_i \perp E_s$  configuration to that in the  $E_i \parallel E_s$  thus can serve as a measure of the change of the relative contribution of this symmetry component in the measured spectra. For nanocrystalline materials the symmetry selection rule of first-order Raman scattering does not hold, and the change in polarization of scattered light may instead indicate the extent of disorientation of the nanocrystallites. The values of  $\rho_D$  for the initial silicon wafer and PS samples are shown in Table II.

The second-order spectrum of transverse (T) acoustical (A) phonons for sample 1 (Fig. 1) is much different from that of  $c$ -Si(111) (Fig. 3) at both polarizations. Peak A, peak C, and a sharp minimum at its right side are no longer clearly observed. Near  $300 \text{ cm}^{-1}$ , the position of peak B, two extremely wide peaks with centers at about  $305$  and  $335 \text{ cm}^{-1}$  are present. We assume that the former is due to TA overtones at  $X$  and  $\Sigma$  critical points as in the case of  $c$ -Si, and the latter comes from an amorphous phase. For sample 2 (Fig. 2), peak A appears to be at its  $c$ -Si position and is more enhanced at both polarization configurations. Peak B emerges above a humplike structure and for  $E_i \parallel E_s$  exhibits a large low-energy shift and much less broadening than for sample 1. With  $E_i \perp E_s$  it has about the same position and width as for  $c$ -Si [Fig. 3(b)].

In Fig. 5 we show a detailed view of the second-order scattering arising from overtones of optical phonons (peak H) at the critical point  $X$ , which forms its left side, at points  $W$ ,  $Q$ ,  $\Sigma$ , and  $S_j$ , which form its left shoulder; at point  $L$ ,

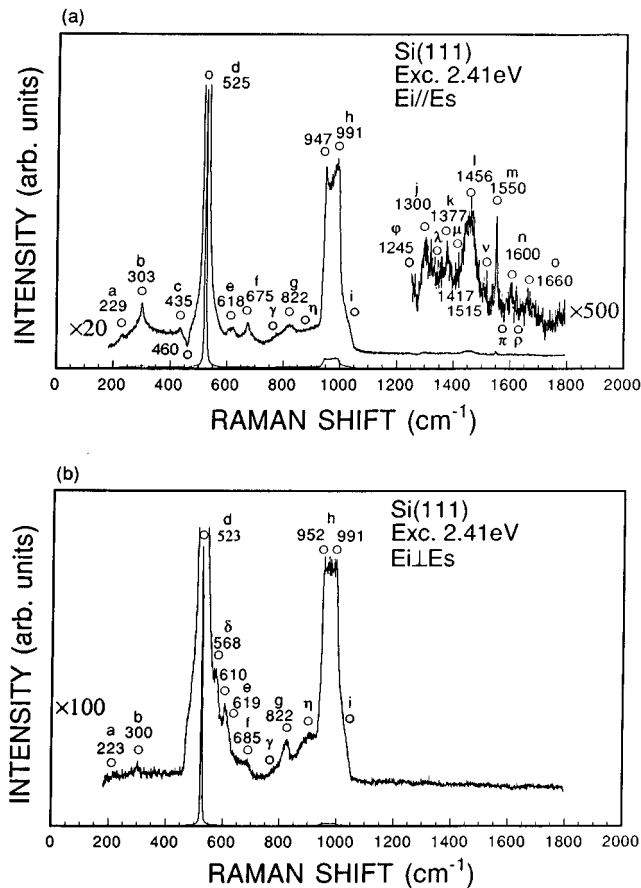


FIG. 3. Raman spectra of the initial Si(111) single-crystal wafer used for preparation of porous silicon samples obtained at 10 K for (a)  $E_i \parallel E_s$  and (b)  $E_i \perp E_s$  (Ref. 44).

which forms its right shoulder, and at  $\Gamma$ , which is responsible for the spectral shape at the bottom of its right side (feature  $I$ ), for porous Si and initial  $c$ -Si. Relevant spectral parameters are presented in Table III. In the spectra at both polarizations for sample 1 this peak completely lost its initial characteristic form, and is much broader than for  $c$ -Si. Its center is close to the position of the left shoulder of this peak for  $c$ -Si. Though its shape can be well described by a Lorentzian, small discontinuities of the slope at about 920 and 970  $\text{cm}^{-1}$  are seen which points to contributions having topological natures of  $2\text{TO}(X)$  and  $2\text{TO}(L)$  modes,<sup>48</sup> respectively. For sample 2 peak  $H$  shows a similar low-energy shift when  $E_i \parallel E_s$  [Fig. 5(a)], but its shape resembles that of the initial  $c$ -Si and the broadening is less. For the  $E_i \perp E_s$  configuration it is barely detectable above the background, and located at about the same position as in  $c$ -Si.

The scattering between peaks  $D$  and  $H$  is composed of contributions from combinations and also from overtones of longitudinal ( $L$ ) phonons (Table I). For sample 1, in the region where  $c$ -Si exhibits two distinct peaks  $E$  and  $F$  (with the main contribution to the latter one in the form of a sharp maximum coming from accidental critical points), a wide feature which we designated here as  $E, F$  arises with a maximum at 632  $\text{cm}^{-1}$ , the position between peaks  $E$  and  $F$  for the initial  $c$ -Si. Peak  $G$  seems to have an intensity diminished to the level of a weaker structure  $\gamma$  on its left side. This results in a shoulderlike feature at 795  $\text{cm}^{-1}$  with  $E_i \parallel E_s$ , and

at 781  $\text{cm}^{-1}$  with  $E_i \perp E_s$ . For sample 2, contributions from peaks  $E$  and  $F$  do not overlap, and the latter has a weaker intensity. Both peaks are notably low energy shifted for  $E_i \parallel E_s$  with centers at 601 and 642  $\text{cm}^{-1}$ , respectively, and for  $E_i \perp E_s$  they remain at approximately the  $c$ -Si positions of 619 and 680  $\text{cm}^{-1}$ , respectively. Peak  $G$  for the  $E_i \parallel E_s$  configuration transforms in the way described for sample 1. For  $E_i \perp E_s$  the structure on its left side  $\gamma$  weakens as well, and peak  $G$  appears as a small feature at about 810  $\text{cm}^{-1}$ ; the value is again close to its  $c$ -Si frequency.

The neighboring bulk of scattering  $\eta$  arising from around 850–920  $\text{cm}^{-1}$  originates from many two-phonon combinations at  $\Sigma$ ,  $L$ , and  $X$  critical points, together with those from three-phonon combinations at  $X$  and  $W$  and  $Y$  and  $L$  critical points, Table I; note that three-phonon scattering is much intensified for porous Si, and from the overtone  $2\text{TO}(2\Sigma)$  is strongly increased in comparison with  $c$ -Si. The intensity of the resulting scattering have become comparable to that from the  $2\text{O}(\Gamma)$  mode (feature  $I$ ) as most easily seen in Fig. 5.

A strong enhancement of multiphonon features occurs for porous silicon, especially for sample 1. Results of a comparison of the spectra in Figs. 1 and 2 with corresponding spectra in Fig. 3 are summarized in Table II. The intensities of peaks  $H$  and  $E, F$  are normalized to those of peak  $D$  there. A strong intensification of peak  $E, F$  takes place. It is extremely enhanced for the perpendicular scattering configuration, and has become even more intense than peak  $H$ . For sample 2 intensification of peaks  $E$  and  $F$  in both polarizations is rather insignificant, as well as that of peak  $H$ , which occurs only for  $E_i \parallel E_s$ .

The third- and fourth-order scattering intensifies and transforms as well. For both porous silicon samples the features broaden to form wider bands, especially for the fourth-order scattering (features  $M-O$ ). There is a strong polarization dependence of their enhancement as shown in Table IV.

In addition to the peaks which can be attributed to the scattering from crystalline material and were described above, all spectra of our porous silicon samples, although to different extents, exhibit broadbands which are characteristic of an amorphous phase. For sample 1, features that resemble the spectrum of pure amorphous silicon consisting of wide bands of TA, LA, LO, and TO phonons<sup>49</sup> (labeled in Figs. 1 and 2 by black circles), respectively, are as follows: the rise in scattering at frequencies lower than 200  $\text{cm}^{-1}$ , the wide band centered at around 335  $\text{cm}^{-1}$ , shoulders of the first-order peak at around 400 and 470  $\text{cm}^{-1}$ , and a minima or breaks in the slope of scattering between the above features and bands from  $2\text{LA}$  and  $2\text{TO}$  phonons (they are of weaker intensity in comparison with other bands,<sup>49</sup> and are hidden by peaks  $E, F$ , and  $H$ , respectively) at around 240, 370, 450, 570, and 750  $\text{cm}^{-1}$ . In both scattering configurations the amorphouslike component is present to an approximately equal extent. For sample 2 this component is enhanced for  $E_i \parallel E_s$ , resulting in clear bands at 340, 420, and 470  $\text{cm}^{-1}$ . However, the bands are very weak for  $E_i \perp E_s$ .

## DISCUSSION

The first-order spectrum from bulk Si single crystal represents scattering by optical phonons with quasimomentum  $\mathbf{q}=\mathbf{0}$  because of its conservation in an infinite lattice. Studies

TABLE I. Phonon assignment of multiphonon Raman features for the initial bulk Si substrates used for preparation of porous Si samples. Denotations of the modes are explained in the text.

Spectral feature designation	Position of feature <sup>a</sup> (cm <sup>-1</sup> )	Critical-point assignment according to:				Calculated frequency <sup>b</sup> (cm <sup>-1</sup> )	
		Ref. 47	Previous studies		Present work		
			Ref. 48	Ref. 68			
<i>a</i>	229	2TA(L)	2TA(L)	2TA(L)	2TA(L)		
<i>b</i>	303	2TA(X)	2TA(X)	2TA(X)	2TA(X)		
	306			2TA2( $\Sigma$ )	2TA2( $\Sigma$ )		
<i>c</i>	435	2TA(W) or 2TA( $\Sigma$ )	2TA( $\Sigma$ )	2TA(W) and 2A1(Q)	2A2(W) 2A1(Q)		
	460		2TA( $\Sigma$ )	2A1( $\Sigma$ ) 2A1(L-K)	2TA1( $\Sigma$ ) 2A1(L-K)		
	525	$O(\Gamma)$	$O(\Gamma)$	$O(\Gamma)$	$O(\Gamma)$		
<i>e</i>	618	TO(X)+TA(X)	$O(\Sigma)$ +A( $\Sigma$ )		TO(X)+TA(X)	617	
	624				LO( $\Sigma$ )+TA1( $\Sigma$ )		
	636				LO( $\Delta$ )+TA( $\Delta$ )		
<i>f</i>	675	TO( $\Sigma$ )+TA( $\Sigma$ ), TO(W)+TA(W) or LO(X)+2TA(L)	accidental critical points		accidental critical points TO2( $\Sigma$ )+TA1( $\Sigma$ ) $O$ 1(W)+A2(W) 2O2(W) TO1( $\Sigma$ )+TA1( $\Sigma$ )	675 690 691 698 705	
	$\gamma$				$O(\Gamma)$ +2TA(L) TA(X)+TA(L)+TO(L) 2TA(X)+TO(X) 2LO( $\Sigma$ )	754 763 768 788	
	<i>g</i>	822	TO+LA or $O(\Gamma)$ +2TA(X)		$O$ 1(W)+ $O$ 2(W) 2L(X) $O(\Gamma)$ +2TA(X)	823 824 828	
	<i><math>\eta</math></i>	850–920				2LO(L) TO2( $\Sigma$ )+LO( $\Sigma$ ) TO1( $\Sigma$ )+LO( $\Sigma$ ) TO(L)+LA(L) TO(X)+L(X) L(X)+2A2(W) TA(X)+2A1(W) TA(X)+2LA(L) TO(X)+2A2(W) L(X)+LA(L)+TA(L)	852 854 869 870 877 847 850 900 900 901
		920				2TO2( $\Sigma$ )	
<i>h</i>		930	2TO(X)	2TO(X)	2TO(X)	2TO(X)	
		947		2TO(W)	2TO(W)	2O1(W) 2O(Q)	
		950			2O( $S_T$ )	2O( $S_T$ ) 2TO1( $\Sigma$ )	
<i>i</i>		991	2TO(L) and 2TO( $\Sigma$ )	2TO(L)	2TO(L)	2TO(L)	991
		1050	2O( $\Gamma$ )	2O( $\Gamma$ )		2O( $\Gamma$ )	1050
$\iota$		1110				L(X)+2O2(W)	1110
		$\varphi$	1245			L(X)+O1(W)+O2(W) 3L(X) L(X)+2LO(L) O( $\Gamma$ )+2LA(L)	1235 1236 1264 1273
			<i>j</i>	1300	2LO(L)+TO(X)		L(X)+TO(L)+LA(L) TO(X)+O1(W)+O2(W) TO(X)+2L(X) TO1( $\Sigma$ )+O1(W)+O2(W)
$\lambda$	1335				L(X)+LO(L)+TO(L) TO(X)+LA(L)+TO(L)	1334 1335	

TABLE I. (Continued).

Spectral feature designation	Position of feature <sup>a</sup> (cm <sup>-1</sup> )	Critical-point assignment according to:			Calculated frequency <sup>b</sup> (cm <sup>-1</sup> )
		Previous studies		Present work	
		Ref. 47	Ref. 48		
<i>k</i>	1377	TO(L)+LO(L)+TO(X) or 3TO(X)		$O(\Gamma) + 2LO(L)$	1377
<i>μ</i>	1417			$O(\Gamma) + TO(X) + L(X)$	1402
				$L(X) + 2TO(L)$	1403
				$TO(X) + 2O1(W)$	1412
				$3TO1(\Sigma)$	1425
<i>l</i>	1456	2TO(L)+TO(X) or 3TO( $\Sigma$ )		$TO(L) + 2O1(W)$	1443
				$O(\Gamma) + 2TO(X)$	1455
				$TO(X) + 2TO(L)$	1456
				$O(\Gamma) + 2O1(W)$	1472
				$LO(\Delta) + TA(\Delta) + 2LO(L)$	1488
				$O(\Gamma) + 2TO(L)$	1516
<i>ν</i>	1515			$O(\Gamma) + 2TO(L)$	1516
	<i>m<sup>c</sup></i>	1550		$2LO(L) + A2(W) + O1(W)$	1543
$2TO(X) + TO(X) + TA(X)$				1547	
$2LO(L) + 2O2(W)$				1550	
$LO(\Delta) + TA(\Delta) + 2TO(X)$				1566	
<i>π</i>	1570			$LO(\Delta) + TA(\Delta) + 2O1(W) / 2TO1(\Sigma)$	1583/1586
				$3O(\Gamma)$	1575
<i>n</i>	1600			$2LA(L) + 2LO(L)$	1600
				$TA(X) + TO(X) + 2TO(L)$	1603
<i>ρ</i>	1627			$2L(X) + 2LO(\Sigma)$	1612
				$LO(\Delta) + TA(\Delta) + 2TO(L)$	1627
				$4L(X)$	1648
<i>o</i>	1660			$2LO(L) + 2LO(\Sigma)$	1640
				$2O1(W) / 2TO1(\Sigma) + O1(W) + A2(W)$	1638/1641
				$2O1(W) / 2TO1(\Sigma) + 2O2(W)$	1645/1648
				$2TO2(\Sigma) + 2LA(L)$	1668
				$2L(X) + 2LO(L)$	1676
				$2TO(X) + 2LA(L)$	1678
				$2TO(L) + O1(W) + A2(W)$	1682
				$2TO(L) + 2O2(W)$	1689
				$2O1(W) / 2TO1(\Sigma) + 2LA(L)$	1695/1698

<sup>a</sup>The data are quoted for the parallel scattering configuration.

<sup>b</sup>The frequency of the  $O2(W)$  phonon was estimated from theoretical data of Ref. 57, and for frequencies of  $L(X)$ ,  $LO(L)$ , and  $LA(L)$ , phonon data of infrared measurements of Ref. 58 were used.

<sup>c</sup>For features  $m-o$ , which reflect four-phonon processes, only the most probable processes are selected.

of the morphology and structure of porous Si by transmission electron microscopy (TEM) has revealed the presence of crystalline structures with dimensions on a nanometer scale.<sup>39,40,50-54</sup> The limitation of the translation symmetry leads to relaxation of this selection rule, and phonons with quasimomentum out of the region around the  $\Gamma$  point determined by the size of the crystallite can contribute to the scattering.<sup>55</sup> Due to the decrease in the frequency of optical phonons with  $\mathbf{q}$  in the vicinity of the BZ center, the Raman line of a spectrum from nanocrystalline material is shifted to lower energies and broadened.

A theory has been developed<sup>56,59</sup> in which confinement of the phonon wave function inside a nanocrystalline is represented by weighting the phonon amplitude as a function of direction. The corresponding phonon confinement function can be expressed in a Fourier series, and the Raman spec-

trum is described by integration over phonon Lorentzians weighted by the square of the Fourier transform of the confinement function. The choice of the weighting function is determined mainly by physical assumptions. Different types of weighting functions have been probed.<sup>59</sup> This model has been used by most workers to describe quantitatively the Raman spectra from porous Si.<sup>38,39,41,42,60-62</sup> In most cases a Gaussian was used as the weighting function. However, the spectra obtained in a series of studies<sup>36,63-66</sup> do not match with theoretical predictions. In all these cases the peak shift is about twice or more than that required to fit the predicted relationship with the FWHM. This discrepancy cannot be eliminated by the choice of the nanocrystalline shape. The adoption of the phonon amplitude to be exactly equal to zero at the boundary (with sinc as a confinement function) does not change the relationship between the peak shift and

TABLE II. Enhancement of the Raman scattering from porous silicon in comparison with the initial silicon substrate and depolarization ratio for the first-order scattering.

Peak polarization	First-order scattering $O(\Gamma)$		Second-order scattering normalized to the intensity of the first-order scattering:				Intensity ratio $\rho(D)$ of the $O(\Gamma)$ scattering in the perpendicular polarization to that in parallel polarization
	$D$		$E, F$		$H$		
	parallel	perpendicular	parallel	perpendicular	parallel	perpendicular	
Porous Si sample 1	15	2.4	17	60	4	4	0.5
Porous Si sample 2	90	65	1.5	1.5	1.8		2.4
Si(111)	1	1	1	1	1	1	3.3

FWHM significantly, and leads mainly to a decrease in the diameter of spherical nanocrystallites for a given shape of the spectrum.<sup>42</sup> This theory also does not explain experimental data for Si nanocrystallites covered by hydrogen atoms prepared by magnetron rf sputtering in hydrogen gas.<sup>30</sup> It seems that no broadening of the first-order spectrum occurred for spherelike nanocrystallites with an average diameter of about 25 Å. The low-frequency shift  $\Delta\omega=6\text{ cm}^{-1}$  of the sharp line was explained by a 2% lattice expansion with a decrease in the size of the nanocrystallites.<sup>30</sup>

In addition, the theory worked well for describing line widening with a decrease of the size of Ge nanocrystallites grown in SiO<sub>2</sub> by rf cosputtering.<sup>67</sup> But no coincidence with experimental data for the peak position, which showed a small blueshift, was found. The authors explained this discrepancy by the exertion of a compressive stress on the nanocrystallites, possibly originating from a mismatch of the lattice constants of Ge and SiO<sub>2</sub>. The bulklike character of the first-order line in the topmost layer of porous Si was explained by relaxation of the increased lattice parameter as a result of the replacement of hydrogen by oxygen.<sup>41</sup> An excellent agreement between the fit and the spectrum was achieved by considering the shift due to a uniaxial strain perpendicular to the surface of the porous Si layer, a distribution of nanocrystallites diameters between 20 and 150 Å, and an amorphous background which represents nanocrystallites smaller than 20 Å.<sup>42</sup>

We can assume that the nanocrystallites in sample 1 prepared in aqueous solution have a spherical shape, as was established by electron microscopy studies of porous Si prepared in aqueous-containing solutions.<sup>39,40,50–54</sup> Then, using theoretical data of Ref. 54 and the value for the FWHM of the first-order spectrum for sample 1, we can estimate the characteristic diameter of the nanocrystallites to be about 41 Å. The predicted peak shift for this value of the FWHM is  $\Delta\omega\cong 6\text{ cm}^{-1}$ , and is 3–4  $\text{cm}^{-1}$  smaller than observed experimentally. The incident power density used by us could lead to an additional low-frequency shift of about 2  $\text{cm}^{-1}$  because of sample heating.<sup>41</sup> The insignificant remaining discrepancy of about 1–2  $\text{cm}^{-1}$  we explain by lattice expansion of the nanocrystallites.<sup>7,30,55</sup> The signature of this expansion is also the high-frequency shift of peak *B* with an upper estimate of about 5  $\text{cm}^{-1}$ . This could be interpreted as  $\cong 0.08\%$  lattice expansion in comparison with bulk Si, using data for the pressure dependence of the 2TA(*X*) mode.<sup>68</sup> Thus the main reason for the low-frequency shift of the first-order peak for

sample 1 anodized in aqueous solution is the phonon confinement effect.

For sample 2 prepared in ethanoic electrolyte, the spectral characteristics of the first-order peak depend strongly on polarization. To fit the theoretical relationship between the FWHM and peak shift for the perpendicular scattering configuration, one should assume that the shape of the nanocrystallites is a narrow rod or even a thin slab, rather than a sphere;<sup>59</sup> again this takes into account a possible slight shift and broadening of the line from laser heating.<sup>41</sup> The estimate of the nanocrystallite size through the FWHM gives two different values for  $E_i\perp E_s$  and  $E_i\parallel E_s$ . In the case of columnar structure they are of about 120 and 45 Å, respectively, while the thin-film structure gives 100 Å and less than 30 Å, respectively. The extremely large low-energy shift of the first-order peak in the parallel configuration,  $\Delta\omega=17\text{ cm}^{-1}$ , in comparison with the theoretically predicted value of about 1–2  $\text{cm}^{-1}$ , cannot be accounted for by laser irradiation or the effects of tensile stress. The latter should also shift peaks *A* and *B* upward,<sup>68</sup> which is clearly not the case [Fig. 2(a)]. We consider that this excessive shift could occur due to a lowering of the phonon frequencies for vibrations in the direction perpendicular to the plane of a thin crystalline slab.<sup>69</sup> If we assume that the peak from first-order scattering is caused at  $E_i\parallel E_s$  by the out-of-plane vibrations, and at  $E_i\perp E_s$  by the in-plane vibrations, for its shift  $\Delta\omega=17\text{ cm}^{-1}$  in the former case, a calculation (Fig. 3 of Ref. 69) gives a difference between the frequency of in-plane and out-of-plane modes of about 11.5  $\text{cm}^{-1}$ , a value close to 13  $\text{cm}^{-1}$ , the difference between positions of this peak in our spectra with different polarizations. These explanations are supported by the results of an x-ray-diffraction study, that nanocrystallites composing porous silicon prepared in ethanol containing electrolyte have in general two quite different dimensions, the larger one being oriented perpendicular to the surface [(100)-oriented silicon wafers were used].<sup>7</sup>

Relative enhancement of the multiorder scattering also can serve as a measure of the size of nanocrystallites. The intensification of scattering from porous silicon in the region of 630  $\text{cm}^{-1}$  was attributed in Ref. 66 to the same origin as in microcrystalline silicon, i.e., to relaxation of the symmetry selection rules,<sup>70</sup> and to a surface assistance in Ref. 42. For sample 2, a weaker intensification of peak *H* and especially of peak *E* (Table II) in comparison with sample 1 supports the above conclusion of a larger average size of nanocrystallites in this sample obtained from the FWHM of the first-

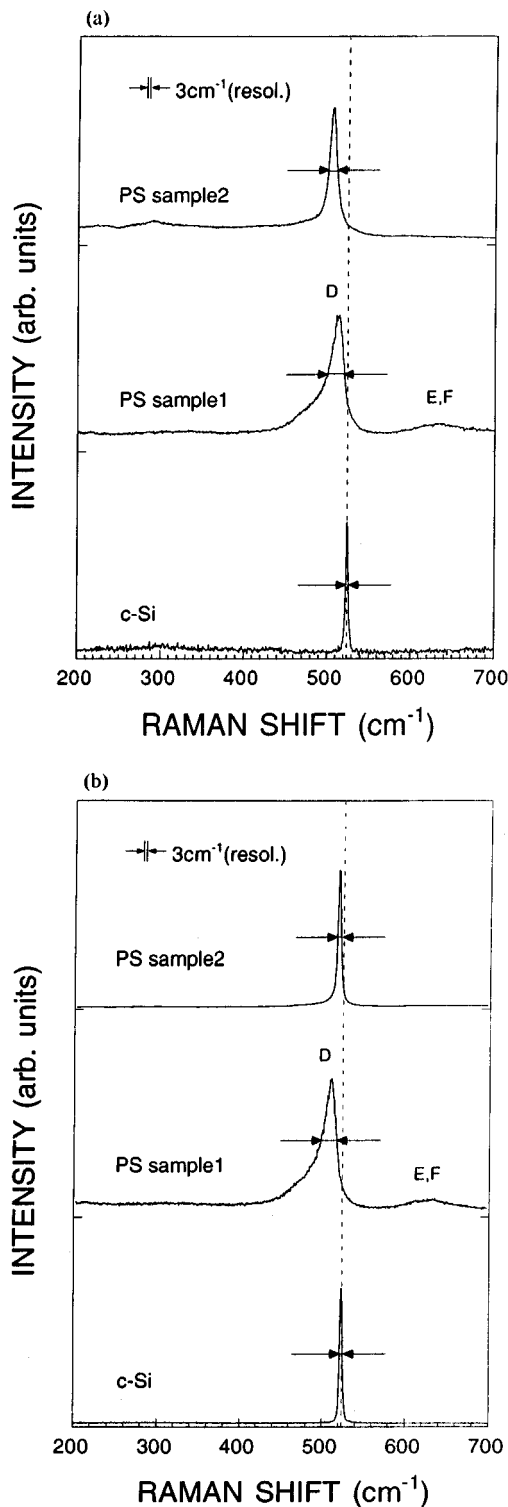


FIG. 4. Detailed view of the Raman spectra in the region of the first-order scattering from porous silicon (PS) samples prepared in aqueous electrolyte (PS sample 1) and ethanoic electrolyte (PS sample 2) compared with that from *c*-Si for (a)  $E_i \parallel E_s$ , and (b)  $E_i \perp E_s$ . Notations correspond to those of Fig. 1.

order scattering. However, the present explanations are tentative, and require further experimental proof, including the use of other imaging techniques like TEM.

The composition of an electrolyte also has strong effect on the morphology of the resulting porous silicon films.

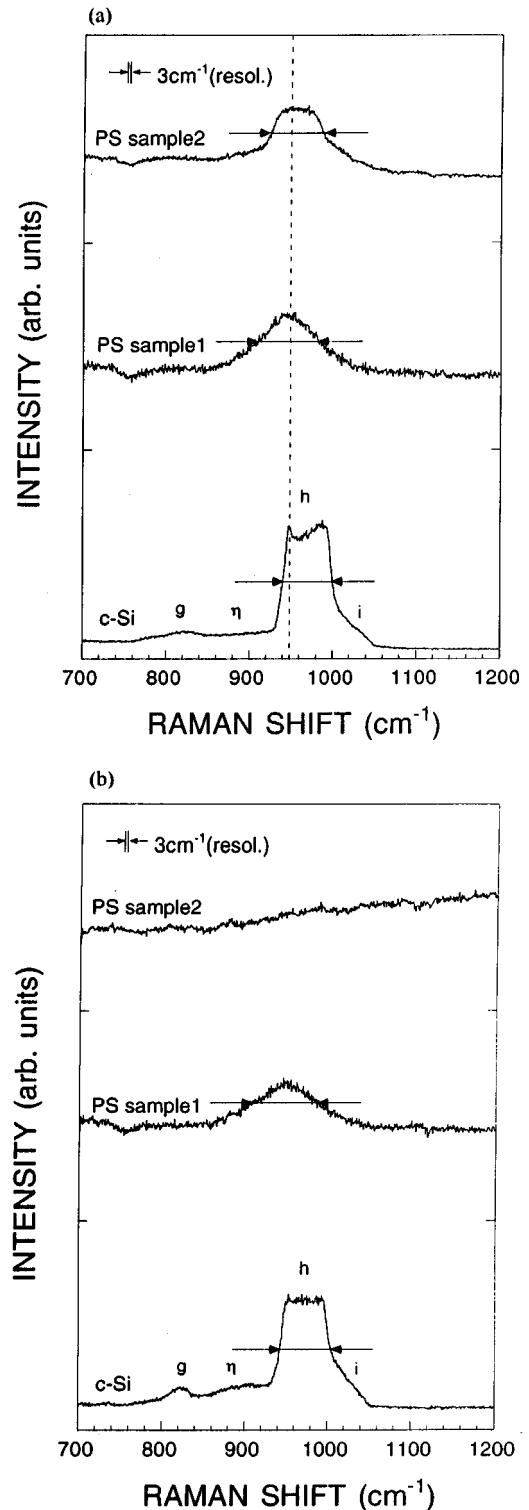


FIG. 5. Detailed view of the Raman spectra in the region of the second-order scattering from overtones of optical phonons from porous silicon (PS) samples prepared in an aqueous electrolyte (PS sample 1) and an ethanoic electrolyte (PS sample 2), compared with that from *c*-Si for (a)  $E_i \parallel E_s$ , and (b)  $E_i \perp E_s$ . Notations correspond to those of Fig. 3.

X-ray studies<sup>6,10</sup> have shown that the microcrystallites in porous Si have a coherent lattice though the whole thickness of the layer, so that they can be viewed as a single crystal. This can be due to the specific mechanism of the anodic etching,

TABLE III. Full width at half maximum (FWHM) and energy shift  $\Delta(w)$  of the first- and second-order scattering from overtones of optical phonons for porous silicon and the initial silicon substrate.

Polarization	First-order scattering (peak $D$ ):				Second-order scattering (peak $H$ ):			
	parallel FWHM ( $\text{cm}^{-1}$ )	$\Delta(w)$ ( $\text{cm}^{-1}$ )	perpendicular FWHM ( $\text{cm}^{-1}$ )	$\Delta(w)$ ( $\text{cm}^{-1}$ )	parallel FWHM ( $\text{cm}^{-1}$ )	$\Delta(w)$ ( $\text{cm}^{-1}$ )	perpendicular FWHM ( $\text{cm}^{-1}$ )	$\Delta(w)$ ( $\text{cm}^{-1}$ )
Si(111)	3.5	0	3.5	0	62	0	64	0
Porous Si sample 1	20	9	20	10	85	23	92	22
Porous Si sample 2	12	17	5	2	72	15		

which results in the propagation of pores along  $\langle 100 \rangle$  crystallographic directions, as was shown by TEM, and it is proposed that this is “a universal property of the formation morphology of porous silicon, independent of dopant type, concentration, or anodization conditions.”<sup>71</sup> Recent high-resolution TEM studies revealed that lattice planes inside microcrystallites of porous silicon prepared in aqueous electrolyte,<sup>53</sup> as well as in an ethanoic electrolyte<sup>52</sup> having in general the same orientations as in the underlying substrate, are misoriented slightly with respect to each other. The degree of misorientation of microcrystallites in our samples

manifests itself in the depolarization ratio  $\rho_D$  of the first-order scattering. For sample 2 anodized in ethanoic electrolyte, its value is much closer to that of the initial  $c$ -Si substrate in comparison with sample 1 (Table II). For sample 1 prepared in an aqueous solution, the value of  $\rho_D$  is close to that of randomly oriented crystallites, which is equal to 0.75.<sup>72</sup> This fact implies a better orientation of nanocrystallites in sample 2, and is in accordance with the extreme rise of the absolute intensity of the Raman scattering from sample 2 in comparison with sample 1. An intensification of the first-order scattering from porous Si has been observed

TABLE IV. Changes in the relative intensity of third- and fourth-order Raman scattering from porous silicon in comparison with the initial silicon substrate.

Polarization	Feature	Porous Si sample 1:		Porous Si sample 2:	
		Position ( $\text{cm}^{-1}$ )	Intensity (qualitatively)	Position ( $\text{cm}^{-1}$ )	Intensity (qualitatively)
Parallel	$\iota$	1110	larger	1110	larger
	$\varphi$	1246	same	1245	same
	$J$	1290	smaller	1300	smaller
	$\lambda$			1337	larger
	$K$	1380	much smaller		
	$\mu$			1417	same
	$L$	1460	much smaller	1460	much smaller
	$\nu$	1510	larger	1510	larger
	$M$	1530	larger	1530	larger
	$\pi$	1575	smaller	1570	same
	$N$	1600	larger	1590	larger
	$\rho$	1615	same	1615	same
	$O$	1660	larger	1660	same
	Perpendicular	$\iota$	1110	larger	1090
$\varphi$		1238	much larger	1245	same
$J$		1310	much larger	1290	same
$\lambda$		1337	same	1343	larger
$K$		1377	little larger		
$\mu$		1417	larger	1417	larger
$L$		1460	larger	1460	larger
$\nu$		1510	larger	1510	larger
$M$		1537	much larger	1536	much larger
$\pi$		1580	much larger	1575	much larger
$N$		1610	much larger	1600	much larger
$\rho$		1640	larger	1620	much larger
$O$		1690	larger	1690	much larger

previously, and credited to surface enhancement or resonance effects.<sup>36</sup> This extreme enhancement is easily seen for the first-order scattering (Table II), and can be explained by the effect of multiple reflections of incident light from better-ordered interfaces inside the porous structure. The above discussion is consistent with the fact that the addition of ethanol to the electrolyte results in better crystallinity and also in a decrease in the strain induced on the substrate from the porous layer.<sup>6</sup> We can associate this decrease in strain with the diminishing of the lattice expansion of porous Si, in accordance with larger dimensions of nanocrystallites<sup>7,30,55</sup> in comparison with samples prepared in aqueous electrolyte.

Assuming that the average size of the nanocrystallites in sample 1 is smaller than in sample 2, we can speculate on the evolution of the phonon density of states, which is reflected by the second-order spectrum with the diminishing of nanocrystallites size. In the region of overtones of acoustical phonons a contribution from the scattering characteristic of amorphous material is present, and complicates the interpretation. The most notable changes there are the disappearance first (Fig. 2) of the scattering from overtones which lead to feature *C*, and then (Fig. 1) a strong diminishing of peak *A*. Peak *F* loses part of its intensity due to accidental critical points at  $675\text{ cm}^{-1}$ , as seen in the spectra for sample 2 (Fig. 2). That is why we consider that the main contribution to peak *E*, *F* of sample 1 actually comes from peak *E* (Fig. 1). The weakly resolved structure on its left side at  $614\text{ cm}^{-1}$  in Fig. 1 corresponds to  $\text{TO}(X)+\text{TA}(X)$ . For this combination no notable deviation from the position for *c*-Si at  $612\text{ cm}^{-1}$  is expected because the frequencies of the  $\text{TA}(X)$  and  $\text{TO}(X)$  phonons change in opposing directions, as can be seen from the shifts of peaks *B* and *H*, respectively. The central peak at  $632\text{ cm}^{-1}$  then probably corresponds to the combination  $\text{LO}(\Delta)+\text{TA}(\Delta)$ , and the break in the slope between these features at  $627\text{ cm}^{-1}$  to the combination  $\text{LO}(\Sigma)+\text{TA}1(\Sigma)$  (Figs. 1 and 4).

The region of overtones of optical phonons (peak *H*) for sample 2 resembles its initial form for *c*-Si, and, as in a previous study,<sup>42</sup> a relative decrease of scattering from overtone  $2\text{TO}(L)$  (right shoulder) as well as of scattering from overtones  $2O(S_i)$  and  $2\text{TO}1(\Sigma)$  (the sharp peak at the left shoulder), takes place [Fig. 5(a)]. A relative contribution from numerous two- and three-phonon modes, which leads to feature  $\eta$  at the left side, and from overtone  $2O(\Gamma)$ , which results in feature *I* at the right side, increases. Further diminishing of crystallite size [the middle spectrum in Figs. 5(a) and 5(b)] leads to a drastic relative decrease of scattering from the  $2\text{TO}(L)$  mode and an extreme relative increase of scattering from the modes which forms features  $\eta$  and *I*. These changes are in general agreement with a decrease of the frequencies of overtones of optical phonons and a broadening of the resulting peak *H*, as has been shown to occur for silicon crystallites of nanometer size.<sup>70</sup>

Our spectra of porous silicon samples show that the relaxation of the symmetry selection rules occurs not only for the first-<sup>42</sup> and second-order<sup>70</sup> Raman processes, but for scattering of higher orders as well. The main contribution to the third- and fourth-order scattering for bulk *c*-Si comes from the  $\Gamma_1$  irreducible symmetry component [this conclusion can be inferred from polarized spectra (Fig. 3) considering that the  $\Gamma_1$  component dominates in the scattering from acoustical

and optical overtones<sup>48,68</sup> and is discussed in details elsewhere.<sup>44</sup> In the porous silicon spectra with  $E_{i\perp}E_s$  [Figs. 1(b) and 2(b)], where the signal of acoustical and optical overtones is diminished, the third- and fourth-order scattering is rather strong, and for sample 2 even exceeds the intensity of the two-phonon spectrum. In addition to the enhancement of the  $\Gamma_1$  component, this intensification could also be caused by enhancement of the scattering associated with other possible  $\Gamma'_{25}$  and  $\Gamma_{12}$  symmetry components (for four-phonon processes in Table I we list only those which contain optical overtones). We should also note that the three- and four-phonon spectrum is much more sensitive to the effects of nanocrystallinity than the scattering of lower orders, as especially seen in the spectra of porous silicon sample 2, which has larger nanocrystallites (Fig. 2). While the peaks of the one- and two-phonon spectrum are still relatively narrow and resemble their shape for bulk *c*-Si, the form of the three- and four-phonon spectrum changes drastically.

Now we will briefly discuss the contribution of the amorphouslike component. The amorphouslike shoulder at  $480\text{ cm}^{-1}$  is seen in all spectra of our porous silicon. The similar broadband with a FWHM of about  $20\text{--}70\text{ cm}^{-1}$  centered around  $470\text{--}500\text{ cm}^{-1}$  has been observed on the low-energy side of the first-order peak in several studies of porous silicon.<sup>62,63,65,73,74</sup> It has also been seen in silicon nanocrystallites prepared by plasma-enhanced chemical vapor deposition,<sup>75</sup> in a hydrogen plasma,<sup>55,76</sup> and by a gas-evaporation technique.<sup>77-79</sup> Several explanations have been proposed. For nanocrystalline silicon this component increases in integrated intensity,<sup>75,77,78</sup> shifts to lower frequencies with decreasing crystallite size,<sup>55,78</sup> and has been attributed to a surfacelike shearing mode of silicon clusters.<sup>55</sup> The Raman spectra of germanium nanocrystallites prepared by a rf cosputtering method<sup>67</sup> and gas-evaporation technique<sup>77,79-81</sup> also showed an analogous amorphouslike peak, but this was explained as a signal from the disordered layer at the surface of the nanocrystallites. A weaker relative contribution of this peak to the spectrum in the former case was accounted for by trapped surfaces of nanocrystallites embedded in the  $\text{SiO}_2$  matrix.<sup>67</sup> Decomposition of the Raman spectra of silicon particles prepared by the gas-evaporation technique even required, introducing a surface mode located at  $435\text{ cm}^{-1}$ .<sup>78</sup> The other amorphous bands at lower frequencies are present in a different proportion to this one. In comparison with sample 1 they are notably enhanced in the  $E_{i\parallel}E_s$  spectrum of sample 2. It was shown for freshly prepared porous silicon that hydrogen atoms are present in the surface layer of the crystallites.<sup>8,9,52</sup> A lattice expansion found for sample 1 can be the result not only of the small crystallite size,<sup>7,55</sup> but of such coverage by hydrogen atoms as well.<sup>30</sup> This passivation may prevent the surface layer from disordering. The nanocrystallites in sample 2 have a larger average size than in sample 1, and hence the pore size should be larger to keep the same value of porosity. This can lead to a faster replacement of hydrogen by oxygen, as our samples were kept at an ambient atmosphere. The insertion of oxygen atoms leads to a relaxation of the lattice expansion<sup>41</sup> and to its distortion,<sup>61</sup> which could result in the relaxation of the Raman selection rules and the appearance of an enhanced amorphouslike component of the spectrum.

However, its strong dependence on polarization (this component is extremely weak in the  $E_i \perp E_s$  spectrum of sample 2) suggests that for thin slablike nanocrystallites it may rather represent the distributions of phonon out-of-plane and in-plane modes sensitive to  $E_i \parallel E_s$  and  $E_i \perp E_s$  polarizations, respectively.

### CONCLUSIONS

In summary, we have observed the low-temperature Raman spectra of free-standing porous silicon. The use of different types of electrolytes for etching silicon substrates, keeping other conditions fixed, resulted in porous films with different morphologies and dimensions of constituent nanocrystallites. When an aqueous solution was used, nanocrystallites with a smaller average size and a spherelike shape were produced. The porous silicon film anodized in an ethanoic solution consists of nanocrystallites which exhibit a spatially dependent confinement of phonons. The differences of

the spectra obtained at parallel and perpendicular scattering configurations point to a thin slablike shape of nanocrystallites. The ordering of the porous structure is better in this case. The sensitivity of the third- and fourth-order scattering to the diminishing of the crystallite size is much higher than that of the lower-order scattering.

### ACKNOWLEDGMENTS

One of the authors (H.T.) thanks H. Okushi, H. Tokumoto, S. Kuroda, K. Kajimura, K. Tanaka, and K. Arai for their continuous support and encouragement. We are grateful to Dr. D. Tweet for critical reading of the manuscript, and to Dr. S. Kuroda, Dr. K. Murata, and R. Takei for their help in the manuscript preparation. This work was partially supported by Nissan Science Foundation, the Akai Foundation, and a Grant-in-Aid for Scientific Research from the Ministry of Education, Science and Culture of Japan.

\*Deceased.

<sup>†</sup>On leave from Faculty of Physics, M. V. Lomonosov Moscow State University, Moscow 117234, Russia.

<sup>‡</sup>On leave from Faculty of Science and Technology, Science University of Tokyo, Noda, Chiba 278, Japan.

<sup>1</sup>A. Uhlir, *Bell Syst. Tech. J.* **35**, 333 (1956).

<sup>2</sup>D. R. Turner, *J. Electrochem. Soc.* **105**, 402 (1958).

<sup>3</sup>G. Bomchil, R. Herino, K. Barla, and J. C. Pfister, *J. Electrochem. Soc.* **130**, 1611 (1983).

<sup>4</sup>M. I. J. Beale, J. D. Benjamin, M. J. Uren, N. G. Chew, and A. G. Cullis, *J. Cryst. Growth* **73**, 622 (1985).

<sup>5</sup>T. Unagami and M. Seki, *J. Electrochem. Soc.* **125**, 1339 (1978).

<sup>6</sup>K. Barla, G. Bomchil, R. Herino, J. C. Pfister, and J. Baruchel, *J. Cryst. Growth* **68**, 721 (1984).

<sup>7</sup>K. Barla, R. Herino, G. Bomchil, J. C. Pfister, and A. Freund, *J. Cryst. Growth* **68**, 727 (1984).

<sup>8</sup>H. Sugiyama and O. Nittono, *J. Cryst. Growth* **103**, 156 (1990).

<sup>9</sup>H. Sugiyama and O. Nittono, *Jpn. J. Appl. Phys.* **28**, L2013 (1989).

<sup>10</sup>I. M. Young, M. I. J. Beale, and J. D. Benjamin, *Appl. Phys. Lett.* **46**, 1133 (1985).

<sup>11</sup>P. Goudeau, A. Naudon, G. Bomchil, and R. Herino, *J. Appl. Phys.* **66**, 625 (1989).

<sup>12</sup>Y. Arita and Y. Sunohara, *J. Electrochem. Soc.* **124**, 285 (1977).

<sup>13</sup>T. Unagami, *J. Electrochem. Soc.* **127**, 476 (1980).

<sup>14</sup>T. Unagami, *Jpn. J. Appl. Phys.* **19**, 231 (1980).

<sup>15</sup>R. W. Hardeman, M. I. J. Beale, D. B. Gasson, J. M. Keen, C. Pickering, and D. J. Robbins, *Surf. Sci.* **152/153**, 1051 (1985).

<sup>16</sup>Y. Kato, T. Ito, and A. Hiraki, *Jpn. J. Appl. Phys.* **27**, L1406 (1988).

<sup>17</sup>G. Bomchil, A. Halimaoui, and R. Herino, *Appl. Surf. Sci.* **41/42**, 604 (1989).

<sup>18</sup>K. H. Kim, G. Bai, M. A. Nicolet, and A. Venezia, *J. Appl. Phys.* **69**, 2201 (1991).

<sup>19</sup>Y. C. Kao, K. L. Wang, B. J. Wu, T. L. Lin, C. W. Nieh, D. Jamieson, and G. Bai, *Appl. Phys. Lett.* **51**, 1809 (1987).

<sup>20</sup>J. Mii, T. L. Lin, Y. C. Kao, B. J. Wu, K. L. Wang, C. W. Nieh, D. N. Jamieson, and J. K. Liu, *J. Vac. Sci. Technol. B* **6**, 696 (1988).

<sup>21</sup>R. Herino, P. Jan, and G. Bomchil, *J. Electrochem. Soc.* **132**, 2513 (1985).

<sup>22</sup>T. Ito and A. Hiraki, *Jpn. J. Appl. Phys.* **26**, 1219 (1987).

<sup>23</sup>T. Ito, T. Yasumatsu, H. Watabe, and A. Hiraki, *Jpn. J. Appl. Phys.* **29**, L201 (1990).

<sup>24</sup>N. Koshida, M. Nagasu, T. Sakusabe, and Y. Kiuchi, *J. Electrochem. Soc.* **132**, 346 (1985).

<sup>25</sup>N. Koshida, H. Koyama, and Y. Kiuchi, *Jpn. J. Appl. Phys.* **25**, 1069 (1986).

<sup>26</sup>N. Koshida, M. Nagasu, K. Echizenya, and Y. Kiuchi, *J. Electrochem. Soc.* **133**, 2283 (1986).

<sup>27</sup>H. Koyama and N. Koshida, *J. Electrochem. Soc.* **138**, 254 (1991).

<sup>28</sup>N. Koshida and K. Echizenya, *J. Electrochem. Soc.* **138**, 837 (1991).

<sup>29</sup>S. Furukawa and N. Matsumoto, *Phys. Rev. B* **31**, 2114 (1985).

<sup>30</sup>S. Furukawa and T. Miyasato, *Phys. Rev. B* **38**, 5726 (1988).

<sup>31</sup>L. T. Canham, *Appl. Phys. Lett.* **57**, 1046 (1990).

<sup>32</sup>V. Lehmann and U. Gösele, *Appl. Phys. Lett.* **58**, 856 (1991).

<sup>33</sup>N. Koshida and H. Koyama, *Jpn. J. Appl. Phys.* **30**, L1221 (1991).

<sup>34</sup>S. R. Goodes, T. E. Jenkins, M. I. J. Beale, J. D. Benjamin, and C. Pickering, *Semicond. Sci. Technol.* **3**, 483 (1988).

<sup>35</sup>K. Inoue, K. Maehashi, and H. Nakashima, *Superlatt. Microstruct.* **12**, 77 (1992).

<sup>36</sup>R. Tsu, H. Shen, and M. Dutta, *Appl. Phys. Lett.* **60**, 112 (1992).

<sup>37</sup>T. Asano, K. Higa, S. Aoki, M. Tonouchi, and T. Miyasato, *Jpn. J. Appl. Phys.* **31**, L373 (1992).

<sup>38</sup>S.-L. Zhang, Y. Hou, K.-S. Ho, B. Qian, and S. Cai, *J. Appl. Phys.* **72**, 4469 (1992).

<sup>39</sup>Y. Kanemitsu, H. Uto, Y. Masumoto, T. Matsumoto, T. Futagi, and H. Mimura, *Phys. Rev. B* **48**, 2827 (1993).

<sup>40</sup>K. Nakagawa, A. Nishida, T. Shimada, H. Yamaguchi, and K. Eguchi, *Jpn. J. Appl. Phys.* **31**, L515 (1992).

<sup>41</sup>F. Kozlowski and W. Lang, *J. Appl. Phys.* **72**, 5401 (1993).

<sup>42</sup>H. Mündler, C. Andrzejak, M. G. Berger, U. Klemradt, H. Lüth, R. Herino, and M. Ligeon, *Thin Solid Films* **221**, 27 (1992).

<sup>43</sup>H. Tanino and H. Okushi, *Jpn. J. Appl. Phys.* **29**, L2133 (1990).

<sup>44</sup>H. Tanino, A. Kuprin, and H. Deai (unpublished).

<sup>45</sup>D. E. Aspnes and A. A. Studna, *Phys. Rev. B* **27**, 985 (1983).

- <sup>46</sup>W. C. Dash and R. Newman, *Phys. Rev.* **99**, 1151 (1955).
- <sup>47</sup>W. P. Acker, B. Yip, D. H. Leach, and R. K. Chang, *J. Appl. Phys.* **64**, 2263 (1988).
- <sup>48</sup>P. A. Temple and C. E. Hathaway, *Phys. Rev. B* **7**, 3685 (1973).
- <sup>49</sup>D. Bermejo and M. Cardona, *J. Non-Cryst. Solids* **32**, 405 (1979).
- <sup>50</sup>A. G. Cullis and L. T. Canham, *Nature* **353**, 335 (1991).
- <sup>51</sup>M. W. Cole, J. F. Harvey, R. A. Lux, and D. W. Eckart, *Appl. Phys. Lett.* **60**, 2800 (1992).
- <sup>52</sup>V. Lehmann, B. Jobst, T. Muschik, A. Kux, and V. Petrova-Koch, *Jpn. J. Appl. Phys.* **32**, 2095 (1993).
- <sup>53</sup>A. Nakajima, Y. Ohshima, T. Itakura, and Y. Goto, *Appl. Phys. Lett.* **62**, 2631 (1993).
- <sup>54</sup>A. Kuprin, N. Ishikawa, K. Furuya, and T. Saito, *Proceedings of the 3rd Japan International SAMPE Symposium* (Materials Research Society of Japan, Tokyo, 1993).
- <sup>55</sup>Z. Iqbal and S. Veprek, *J. Phys. C* **15**, 377 (1982).
- <sup>56</sup>H. Richter, Z. P. Wang, and L. Ley, *Solid State Commun.* **39**, 625 (1981).
- <sup>57</sup>W. Weber, *Phys. Rev. B* **15**, 4789 (1977).
- <sup>58</sup>F. A. Johnson and R. Loudon, *Proc. R. Soc. London Ser. A* **281**, 274 (1964).
- <sup>59</sup>I. H. Campbell and P. M. Fauchet, *Solid State Commun.* **58**, 739 (1986).
- <sup>60</sup>Z. Sui, P. P. Leong, P. Herman, G. S. Higashi, and H. Temkin, *Appl. Phys. Lett.* **60**, 2086 (1992).
- <sup>61</sup>J. C. Tsang, M. A. Tischler, and R. T. Collins, *Appl. Phys. Lett.* **60**, 2279 (1992).
- <sup>62</sup>A. Nakajima, Y. Nara, Y. Sugita, T. Itakura, and N. Nakayama, *Jpn. J. Appl. Phys.* **32**, 415 (1993).
- <sup>63</sup>J. M. Perez, J. Villalobos, P. McNeill, J. Prasad, R. Cheek, J. Kelber, J. P. Esterera, P. D. Stevens, and R. Glosser, *Appl. Phys. Lett.* **61**, 563 (1992).
- <sup>64</sup>A. K. Sood, K. Jayaram, and D. Victor S. Muthu, *J. Appl. Phys.* **72**, 4963 (1992).
- <sup>65</sup>H.-J. Lee, Y. H. Seo, D.-H. Oh, K. S. Nahm, E.-K. Suh, Y. H. Lee, H. J. Lee, Y. G. Hwang, K.-H. Park, S. H. Chang, and E. H. Lee, *Appl. Phys. Lett.* **62**, 855 (1993).
- <sup>66</sup>H. D. Fuchs, M. Stutzmann, M. S. Brandt, M. Rozenbauer, J. Weber, A. Breitschwerdt, P. Deak, and M. Cardona, *Phys. Rev. B* **48**, 8172 (1993).
- <sup>67</sup>M. Fujii, S. Hayashi, and K. Yamamoto, *Jpn. J. Appl. Phys.* **30**, 687 (1991).
- <sup>68</sup>B. A. Weinstein and G. J. Piermarini, *Phys. Rev. B* **12**, 1172 (1975).
- <sup>69</sup>G. Kanellis, J. F. Morhange, and M. Balkanski, *Phys. Rev. B* **21**, 1543 (1980).
- <sup>70</sup>P. M. Fauchet, in *Light Scattering in Semiconductor Structures and Superlattices*, edited by D. J. Lockwood and J. F. Young (Plenum, New York, 1990).
- <sup>71</sup>S.-F. Chuang, S. D. Collins, and R. L. Smith, *Appl. Phys. Lett.* **55**, 675 (1989).
- <sup>72</sup>R. J. Kobliska and S. A. Solin, *Phys. Rev.* **8**, 756 (1973).
- <sup>73</sup>Y. H. Seo, H.-J. Lee, H. I. Jeon, D. H. Oh, K. S. Nahm, Y. H. Lee, E.-K. Suh, H. J. Lee, and Y. G. Kwang, *Appl. Phys. Lett.* **62**, 1812 (1993).
- <sup>74</sup>T. Tamura, A. Takazawa, and M. Yamada, *Jpn. J. Appl. Phys.* **32**, L322 (1993).
- <sup>75</sup>E. Bustarret, M. A. Hachicha, and M. Brunel, *Appl. Phys. Lett.* **52**, 1675 (1988).
- <sup>76</sup>S. Veprek, Z. Iqbal, H. R. Oswald, and A. P. Webb, *J. Phys. C* **14**, 295 (1981).
- <sup>77</sup>S. Hayashi and H. Abe, *Jpn. J. Appl. Phys.* **23**, L824 (1984).
- <sup>78</sup>T. Okada, T. Iwaki, K. Yamamoto, H. Kasahara, and K. Abe, *Solid State Commun.* **49**, 809 (1984).
- <sup>79</sup>S. Hayashi and K. Yamamoto, *Superlatt. Microstruct.* **2**, 581 (1986).
- <sup>80</sup>S. Hayashi, M. Ito, and H. Kanamori, *Solid State Commun.* **44**, 75 (1982).
- <sup>81</sup>S. Hayashi, H. Wakayama, T. Okada, S. S. Kim, and K. Yamamoto, *J. Phys. Soc. Jpn.* **56**, 243 (1987).